2 CODA CHARACTERISTICS

2.1 INTRODUCTION

From the geological point of view, it is evident that the earth has heterogeneities on many scales. Rocks have crystals that range in size from fractions of mm to a few cm in scale. An example is in Figure 2-1 where a picture of granite is shown.

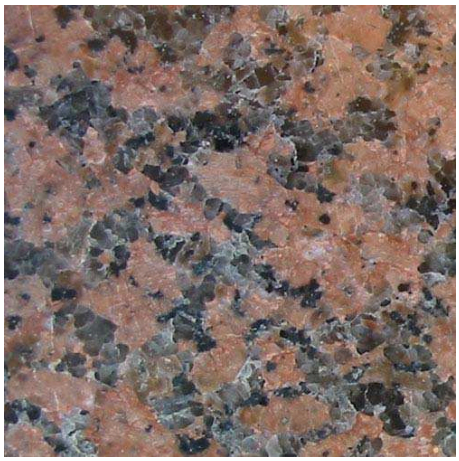

Figure 2-1. Picture of the crystals of granite [6].

Also, fractures range in size from submicroscopic to many tens of meters. Faults can be larger than 1000 km as S. Andreas Fault (see Figure 2-2).

Figure 2-2. S. Andreas Fault, California [7].

Additionally, the earth's crust contains a wide variation of rock types; its composition can range on scales of a few mm to many km. Tectonic processes also contribute to heterogeneity in the lithosphere by means of faulting and folding.

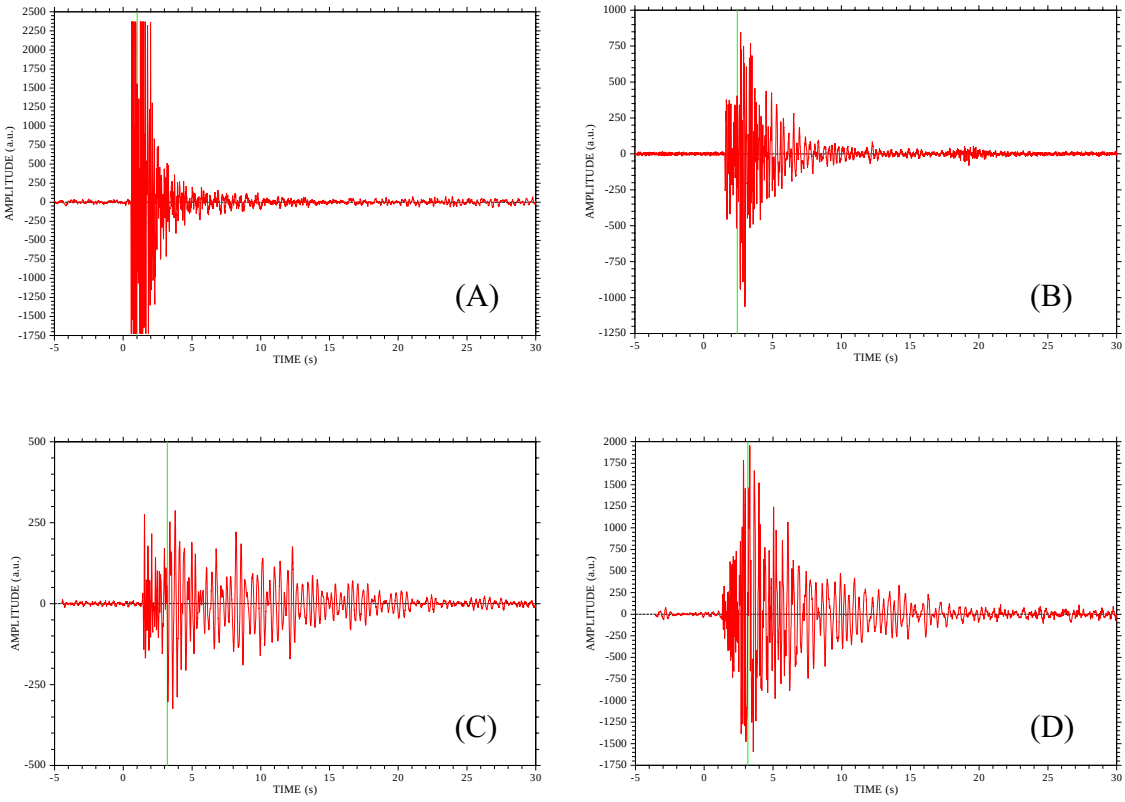

Figure 2-3. Non-filtered seismograms corresponding to Galeras volcano events (appendix A). (A) Event 4 station 22, 26/09/1989. (B) Event 75, station 4, 02/06/1992 (C) Event 250 station 19, 16/02/1996, (D) Event 301, station 20, 30/04/1997. Green lines indicate the S-waves arrival time.

Ground motion in the vicinity of earthquakes often dies away slowly leaving a tail following the passage of primary waves. Aki [8] called the observed continuous wave trains "coda waves" and this term has been used since then to describe the tail portion of regional seismograms.

Examples of coda waves following the primary waves corresponding to events in the Galeras volcano (that will be studied in Chapter 6) are shown in Figure 2-3. At present, the word "coda" is used to refer all wave trains except direct waves, thus naming P-coda the waves between the direct P and S waves and S-coda the waves following the direct S-waves. Because the most prominent characteristic of typical high

frequency seismograms of local earthquakes is the coda of S-waves, in this work we will use the word coda for the S-wave coda.

Aki (1969) [8] proposed that the coda was the result of the scattering of seismic waves by random heterogeneities in the earth's lithosphere. Therefore, the later portion of regional seismograms may be considered as a result of some kind of averaging over many samples of heterogeneities, thus suggesting a statistical treatment in which a small number of parameters characterize the average properties of the heterogeneous medium.

Aki and Chouet (1975) [9] developed two simple theoretical models that proved to fit extremely well the observed energy envelopes of coda waves: the single scattering model and the diffusion model. The first one relied on the simple assumption that waves are scattered only once on their way from the source to the station. On the other hand, the second describes the coda by means of a diffusion equation. They also introduced coda Q (Q_c) as a parameter to account for anelastic loss of energy from the wavefield. Q_c, which describes the rate of decay of seismogram envelopes, has been extensively measured in many regions of the world [10] and it has proved to be an extremely sensitive parameter to the geological environment. Both the single scattering and the diffusion models will be developed in detail in section 2.4.

The physical interpretation of Q_c in terms of the medium properties still remains unclear. Within the context of the single scattering theory, Q_c appears to represent an effective total attenuation including both absorption and scattering loss:

$$\frac{1}{Q_c} = \frac{1}{Q_t} = \frac{1}{Q_s} + \frac{1}{Q_i} \tag{2.1}$$

where Q_t, Q_s and Q_i denote the total, scattering and intrinsic quality factors, respectively. On the other hand, in the diffusion model Q_c represents the effect of absorption only ($Q_c = Q_i$). In order to give a meaningful interpretation to Q_c, it is therefore critical to determine the range of validity of the various approximations used to fit the data. The radiative transfer theory is the tool that can address this problem. This theory enables the calculation of energy envelopes of seismic waves taking into account all orders of scattering. Radiative transfer was first introduced in Seismology by Wu [11] and it has, since then, greatly enhanced the understanding of the coda of

earthquakes. Radiative transfer theory shows a different functional dependence for Q_s and Q_i. This makes it possible to determine both magnitudes from total attenuation (Frankel and Wennerberg, 1987 [12]; Hoshiba et al., 1991 [13]]; Matsunami, 1991 [14]),

The most sophisticated modelling one may hope for is the complete fitting of seismic waveforms, which contain all information on phase and amplitude. The goal of the radiative transfer (and the other models commented above) is more modest as they aim at explaining only the energy envelope of the seismograms. However, at relatively high frequencies, the correlation length of the wavefield is of the order of a few kilometres only (Dainty and Toksöz, 1990 [15]), which makes the waveform fitting procedure almost inapplicable. In disordered media or random media the phase gets randomized by the scattering events. As a consequence, the wavefield at a point can be viewed as a sum of waves whose phase and amplitude are independent random variables. We may then reasonably expect that wave energies rather than amplitudes are additive in random media. But, since on the time scale of seismic observations the Earth is a static disordered medium we do not have access to a true statistical ensemble. In other words, scattering is a deterministic process that happens at cracks, inhomogeneities, faults…, not a stochastic process [16]. Thus, theory and observation can only be connected through some kind of ergodic hypothesis (time average and space average coincide).

2.2 S-WAVE CODA ATTRIBUTES

Let us first enumerate several important observations about the coda waves, which were compiled by Aki and Chouet [9] and that may be satisfactorily explained by a "backscattering model":

A. The spectral contents of the early part of a local earthquake seismogram depend strongly on the travel distance and the nature of the wave path to a station. The difference in spectrum among stations, however, diminishes in the later part of the seismograms and disappears in the coda.

B. The coda length is nearly independent of the epicentral distance or azimuth for a

given region and can be used effectively as a measure of earthquake magnitude.

C. The power spectra of coda waves from different local earthquakes decay as a function of time in the same manner at all stations and for all events within a given region. The temporal decay shape is independent of earthquake magnitude for events with local magnitudes (M_L) less than about 6.

D. The coda amplitude varies with the local geology at a recording site. It can be 5-8 times larger on the sediment than on granite. Interestingly, the amplitude of ambient ground noise tends to be proportional to the site factor of coda excitation, making the total duration nearly independent of local geology.

E. The study of coda by a small-aperture array seismographs shows that they are not regular plane waves from the epicenter.

Now let us now follow the waves as they are generated when an earthquake occurs. An important initial consideration is that we expect that the source duration of earthquakes with M_L<6 is less than a few seconds. This consideration is supported by the fact that the duration of the major event at an earthquake source may be measured roughly by the fault length divided by the rupture velocity, where the fault length for earthquakes with magnitude M_L~6 is about 10 km and the rupture velocity is roughly the shear velocity. Similarly, the duration for an M_L~1 earthquake is probably a few hundredths of a second.

Then, the nature of the primary waves which spread outward from the source and are recorded at a station will depend on the earth's structure along the wave path from source to station. As the primary waves spread out, secondary waves are generated at each of the heterogeneities that they encounter. Suppose for simplicity, that both the primary and the secondary waves are of the same kind of wave with velocity v. Then we consider a time interval $(t, t+\Delta t)$ measured from the origin where Δt is longer than the duration of primary waves. During this time interval the secondary waves arrive from the heterogeneities within the zone sandwiched by two ellipsoids, both with the foci at source and station and with the length of the major axis equal to vt and $v(t+\Delta t)$. If we consider seismograms of an event recorded at two different stations, for the given time interval $(t, t+\Delta t)$ the two ellipsoidal zones will increasingly overlap as t increases.

Besides, a greater number of heterogeneities will contribute to the later time interval and tend to average out the difference between backscattering energies received at the two stations. Thus the difference in the appearance of seismograms disappears in the coda.

2.3 CHARACTERIZING S-CODA ENVELOPES

To characterize S-coda envelopes one often calculates the smoothed trace of the square of the seismogram for a narrow frequency band, which is called the MS seismogram envelope. The amplitude of the MS envelope is linearly proportional to energy density. A very important property of the MS envelopes $A^2(f,t)$ (which are a function of frequency f and lapse time t) is that they can be described as the product of the spectrum of waves radiated by the source $S(f)$, and a function describing the response of the medium to a source $\phi(f,t)$ (Aki, 1969 [8]):

$$A^2(f,t) = S(f)\cdot\phi(f,t) \tag{2.2}$$

This relation constitutes a cornerstone in coda-wave analysis and has been confirmed for many different areas (Aki and Chouet, 1975[9]; Rautian and Khalturin, 1978 [17]). The assumption that $\phi(f,t)$ is common to all sources implies that different seismic sources share a common composition of wave types, so that the same scattering effects apply to all. Then, the precise form of $\phi(f,t)$ depends upon how seismic waves are scattered and attenuated.

Two extreme models of scattering are the single scattering, for which outgoing waves are reflected only once before reaching the receiver, and multiple scattering, to the extent that seismic energy is scattered so much that it diffuses away from the source. For both cases, when the time t after the event is large compared with the distance to the source, r, divided by the wave velocities v, ($t>>r/v$), theoretically is $\phi(f,t)$ independent of distance r, and is of the form:

$$\phi(f,t) = t^{-\nu}\exp\left(-\frac{2\pi ft}{Q_c}\right) \tag{2.3}$$

where Q_c is a measure of attenuation. The constant ν takes into account geometrical

spreading and it is equal to 2 for single scattering of body waves. The diffusion theory gives $\nu = 3/2$ (Aki and Chouet, 1975 [8]; Rautian and Khalturin, 1978 [17]) Then, if $A^2(f,t)$ follows Eq. (2.2) and the envelope of the coda is predicted to be and turns out to be independent of the source spectrum $S(f)$, in principle the parameters ν and Q_c can be determined. From them, inferences about how scattering takes place can be made and the properties of different regions can be compared.

A remarkable property of the coda is that at any given station, for each frequency band, the dependence of the envelope of the coda on time is nearly identical for all events in a large region surrounding the station. This was noticed by Rautian and Khalturin (1978) [17] when they represented together data from several different events of different magnitudes in a certain region and obtained parallel lines. If the events were combined without regard to their individual levels, they observed a remarkably good overlapping. When they built a summary of coda envelopes for different frequency bands as a function of time they observed that for each band the scatter among the data was remarkably small, in general less than a factor of 2 (see Figure 2-4). Even when these bands were built from events within 50 km of the station, data from events as far as 600 km from intermediate depths also fell on the bands. They concluded that, at a given station, the time dependence of the envelope of the coda in the frequency band 0.1 to 40 Hz is essentially independent of the location of the source, which justifies the separation of the coda spectrum at a given site into a source factor, which is independent of time, and a path factor which shapes the coda with time.

The above authors also experienced that the amount of time that must transpire before the coda envelopes overlap one another depends on epicentral distance. They observed that if t_S-t_0 is the time between the S-wave arrival time t_S and the origin time t_0, then often after $2(t_s - t_0)$ and always after $3(t_s - t_0)$, the general form of the coda is established.

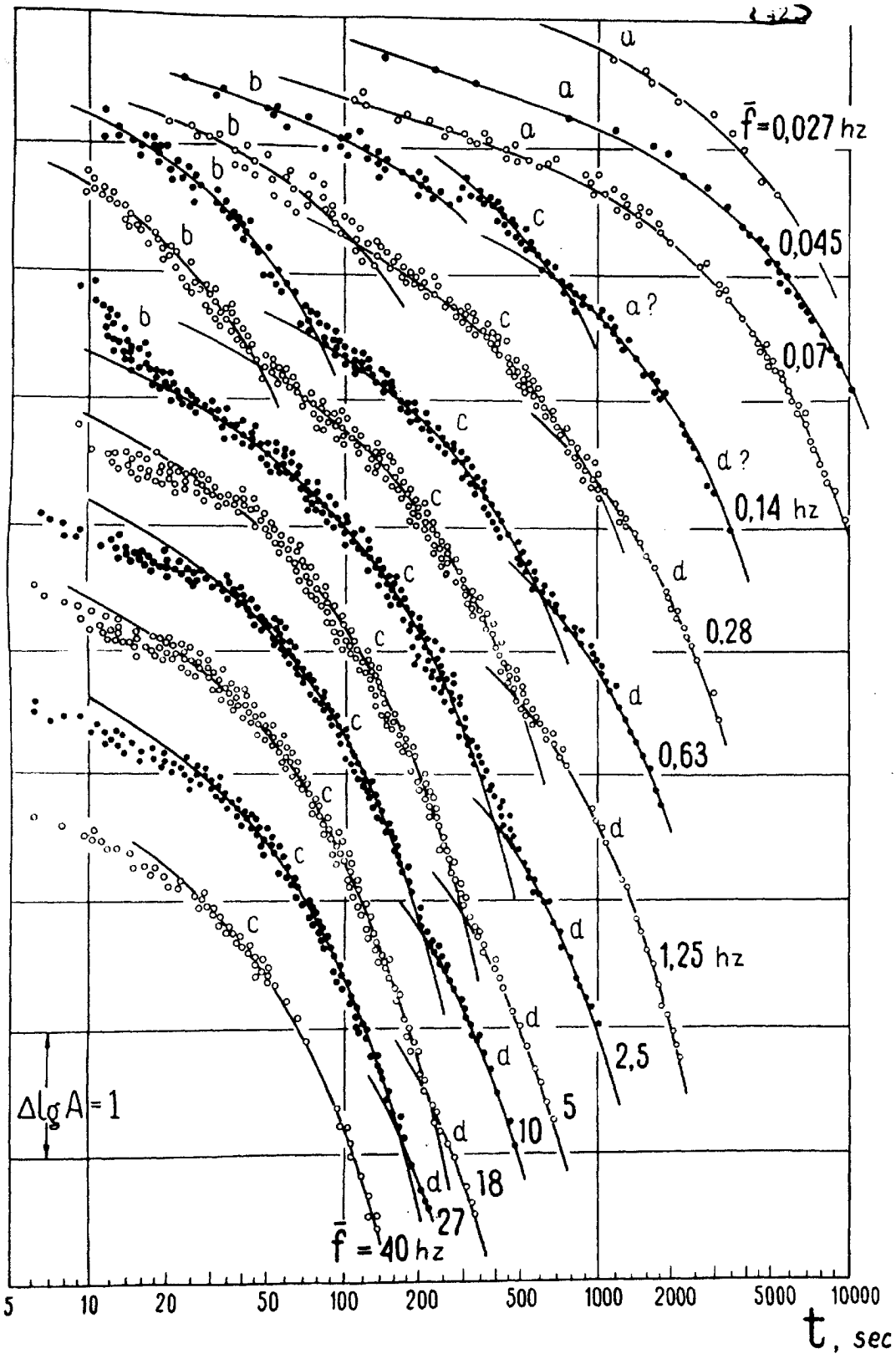

Figure 2-4. Summary of root mean squared coda envelopes for different frequency bands. Data are from many different events [17].

Although the time dependence of the envelope of the coda at a particular station is independent of the position of the earthquake, sometimes the envelopes at different stations from the same earthquake are different in absolute level. This presumably reflects differences in the environments of stations-attenuation and local site effects. The time dependences of the codas for different events differ only by a constant factor for each frequency band. Therefore when a simple correction is applied to the codas at one station, the corrected envelopes overlap the observed envelopes at the other station for all events. This correction is the same for all events independent of the positions of the earthquakes, and therefore epicentral distance. Then, the envelope of the coda over a wide range of frequencies is a very stable function of time and of hypocenter. Rautian and Khalturin (1978) [17] noticed that coda envelopes cannot be described by a single Q_c value, but it changes with different segments and different frequencies. Single scattering coda models that are based on the assumption of spatial homogeneity of the scattering coefficient and intrinsic attenuation predict that Q_c is independent of lapse time. Most of the investigators who found a lapse time dependence of the coda decay rate suggested that the later portion of the coda is dominated by energy that has propagated in zones with lower attenuation than energy in the early coda. However, lapse time dependence of coda decay is still an unresolved issue (Sato and Fehler, 1998) [10].

The frequency dependence of Q_c can be written in the form of a power of frequency f as $Q_c \propto f^n$ for f>1 Hz. The power n ranges between 0.5 and 1.

2.4 TWO EXTREME MODELS FOR CODA WAVES

Several phenomenological models for coda-wave generation have been proposed. Aki and Chouet (1975) [9] proposed the single backscattering model to explain the time dependence of the scattered energy density at the source location in 3-D space. They considered the case of impulsive spherical radiation of total energy from the source, which location was coincident with the receiver.

Sato (1977)[18] extended the formulation for the case of a single isotropic scattering model for general source and receiver locations. Under the single scattering approximation, the coda is considered as a superposition of backscattering wavelets

from discrete scattering sources. Each wavelet is due to a single scatterer in the absence of the other scatterers. Another extreme model is to consider the seismic energy transfer as a diffusion process (Wesley, 1965 [19]; Aki and Chouet, 1975 [9]; Dainty and Toksöz, 1981 [20]).

2.4.1 SINGLE ISOTROPIC SCATTERING MODEL

We are going to consider now how the elastic energy propagates in a three-dimensional infinite elastic medium, in which numerous scatterers are distributed homogeneously and randomly, when the elastic energy is radiated spherically. In other words, we restrict the problem to the body wave isotropic scattering. Then, we will derive a space-time distribution of the mean energy density of the single scattered waves in a similar fashion as the one given by Sato (1977) [18].

2.4.1.1 Distribution of scatterers. Isotropic scattering assumption

We suppose that scatterers are distributed randomly and homogeneously with a number density n in the elastic medium. The scattered waves will be considered as incoherent waves. Scatterers are generally characterized by the effective cross section σ. Here, we notice that σ depends on $\omega = 2\pi f$. When scatterers are distributed homogenously with the number density n, the length

$$l = \frac{1}{n\sigma} \tag{2.4}$$

is the mean free path and l/v the mean free time, being v the wave velocity. The scatterers reduce the mean energy flux density of the incident wave by $\exp(-x/l)$, where x is the distance along the propagation direction. The scattering coefficient (turbidity) corresponds to $g=1/l$ and can be measured. The turbidity is of the order of $10^{-5} \sim 10^{-6}\, m^{-1}$ at frequencies higher than 10 Hz [9].

Here, we will assume isotropic scattering in order to obtain an analytic solution with rather simple calculations. Roughly, isotropic scattering may be assumed when the wavelength $\lambda \approx a$ where a is the size of the scatterers (Sato, 1977, [18]). For the sake of simplicity, no conversion between longitudinal waves and transverse waves during

scattering will be considered and the medium will be characterized by a single wave velocity.

2.4.1.2 Single isotropic scattering approximation

Let us suppose that the mean free path l is much longer than the distance r under consideration $(r \ll l)$ or $(t \ll l/v)$. Since the scattering is assumed to be a weak process, only single scattering is considered. Let us also suppose that the source emit a unit of energy in the time t=0. The mean energy density at a certain distance r_1 may then be written as:

$$E_d(r_1, t = r_1/v)dt = \frac{\exp(-n\sigma r_1)}{4\pi r_1^2} \tag{2.5}$$

where dt is the time it takes to emit the unit energy. Note that E_d is the energy per unit area and per unit time. The amount of energy scattered at a certain volume (dV=dS·dr=dS·v·dt) may then be written as:

$$E_s(r_1, t = r_1/v)vdtdS = \frac{\exp(-n\sigma r_1)}{4\pi r_1^2} \cdot \frac{dr}{l} \cdot dS = \frac{n\sigma \exp(-n\sigma r_1)}{4\pi r_1^2} dV \tag{2.6}$$

where E_s is the energy scattered per unit volume and per unit time. The mean energy flux re-emitted by a certain scatterer (located inside a certain dV at the coordinates $\mathbf{r}_1$) at a point $\mathbf{r}_2$ is then written as:

$$E_s(r,t)vdtdS = \frac{\exp(-n\sigma r_2)}{4\pi r_2^2} \cdot E_s(r_1, t = r_1/v)vdtdS \tag{2.7}$$

where $\mathbf{r} = \mathbf{r}_1 + \mathbf{r}_2$. Using Eq.(2.6) we obtain:

$$E_s(r,t)vdtdS = \frac{n\sigma \exp(-n\sigma(r_1 + r_2))}{(4\pi)^2} \cdot \frac{1}{r_1^2 r_2^2} \cdot dV \tag{2.8}$$

In order to get all the energy scattered in a certain time interval dt we will consider a new set of coordinates (alternate prolate spheroidal coordinates which are adapted to “two-centre” problems [21]):

$$x = a\sqrt{\left(\xi_1^2 - 1\right)\left(1 - \xi_2^2\right)}\cos\xi_3$$
$$y = a\sqrt{\left(\xi_1^2 - 1\right)\left(1 - \xi_2^2\right)}\sin\xi_3$$
$$z = a\xi_1\xi_2 \tag{2.9}$$

$$dV = vdtdS = a^3\left(\xi_1^2 - \xi_2^2\right)d\xi_1 d\xi_2 d\xi_3$$

The set of coordinates (ξ_1, ξ_2, ξ_3) are defined on certain intervals that we write as: $\xi_1 \in [1, \infty)$, $\xi_2 \in [-1, 1]$, $\xi_3 \in [0, 2\pi]$.

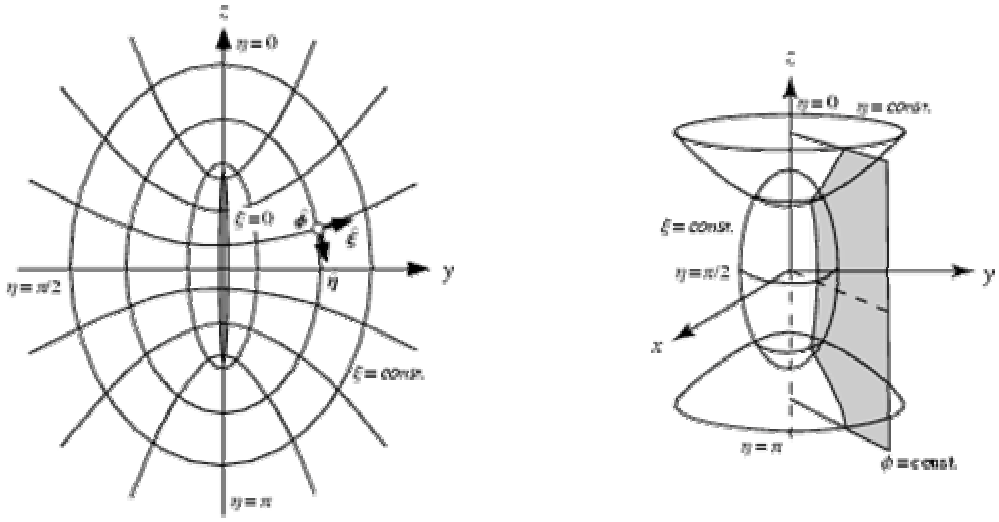

Figure 2-5 Prolate spheroidal coordinates. $\xi_1 = \sinh\xi$, $\xi_2 = \cos\eta$, $\xi_3 = \phi$ [21].

Then we write the coordinates of the source as (0,0,-a), and the ones of the receiver as (0,0,a). Then $\mathbf{r} = (0, 0, 2a)$, $\mathbf{r}_1 = (x, y, z + a)$, $\mathbf{r}_2 = (x, y, z - a)$. Notice the following equalities:

$$r_1 = a\left(\xi_1 + \xi_2\right) \qquad r_2 = a\left(\xi_1 - \xi_2\right) \qquad 2a = \left\|\mathbf{r}_1 + \mathbf{r}_2\right\| = r$$
$$\xi_1 = \frac{r_1 + r_2}{2a} = \frac{vt}{r} \qquad \xi_2 = \frac{r_1 - r_2}{2a} \tag{2.10}$$

where r is the distance from the source to the observer. Notice that:

$$d\xi_1 = \frac{v}{r}dt \tag{2.11}$$

Then dV may be writen as:

$$dV = vdtdS = vdt \cdot \frac{1}{r} a^3 \left(\xi_1^2 - \xi_2^2\right) d\xi_2 d\xi_3 \tag{2.12}$$

and using Eqs. (2.9) , (2.10) and (2.12) in Eq. (2.8) we obtain:

$$E_s(r,t)vdtdS = vdt \frac{n\sigma \exp(-n\sigma)}{(4\pi)^2 r} \frac{1}{a} \frac{1}{\left(\xi_1^2 - \xi_2^2\right)} d\xi_2 d\xi_3 \tag{2.13}$$

Now, integrating the third coordinate:

$$E_s(r,t)vdtdS = vdt \frac{n\sigma \exp(-n\sigma)}{4\pi r^2} \frac{1}{\left(\xi_1^2 - \xi_2^2\right)} d\xi_2 \tag{2.14}$$

and then the second we obtain:

$$E_s(r,t)vdtdS = vdt \frac{n\sigma \exp(-n\sigma)}{4\pi r^2} \frac{1}{\xi_1} \ln\left(\frac{\xi_1 + 1}{\xi_1 - 1}\right) \tag{2.15}$$

Using Eq. (2.10) we may finally write:

$$E_s\left(r,t\right) = \frac{n\sigma \exp\left(-n\sigma vt\right)}{4\pi r} \cdot \frac{1}{vt} \cdot \ln\left(\frac{vt + r}{vt - r}\right) \tag{2.16}$$

2.4.1.3 Properties of the solution

It is important to consider how this distribution behaves for $t \gg r/v$. Considering a first order Taylor expansion of the logarithmic expression we obtain:

$$\frac{r}{vt} \ln\left(\frac{1 + r/vt}{1 - r/vt}\right) \simeq 2\left(\frac{r}{vt}\right)^2 \tag{2.17}$$

Then, for $t \gg r/v$ we may write:

$$E_s(r,t) \simeq \frac{n\sigma \exp(-n\sigma vt)}{2\pi (vt)^2} \tag{2.18}$$

We observe a t^{-2} dependence under such condition, as derived for the single backscattering model of Aki and Chouet (1975) [9].

We notice now that Eq. (2.16) makes sense only for $vt \geq r$. Then we may write:

$$E_s(r,t) = \frac{n\sigma \exp(-n\sigma vt)}{4\pi r} \cdot \frac{1}{vt} \cdot \ln\left(\frac{vt+r}{vt-r}\right) \theta(vt-r) \tag{2.19}$$

This distribution diverges for $vt \to r$. The total energy scattered up to a certain time t may be written as:

$$U(t) = \int_0^{\infty} E_s(r,t) 4\pi r^2 dr = \frac{n\sigma \exp(-n\sigma vt)}{vt} \cdot \int_0^{vt} r \cdot \ln\left(\frac{vt+r}{vt-r}\right) dr \tag{2.20}$$

and solving the integral it yields:

$$U(t) = n\sigma vt \exp(-n\sigma vt) \tag{2.21}$$

Notice that this expression does not tend to one for $t \to \infty$; it tends to zero. The expressions previously developed are only valid for $t \ll l/v$. This means that as time increases, the energy coming from double scattering becomes smaller.

2.4.2 RATIO OF SINGLE SCATTERED ENERGY VERSUS MULTIPLE SCATTERED ENERGY

Equation (2.19) gives us the distribution of energy that arrives at the distance *r* at the time *t* after a single scattering process. Equation (2.21) gives us the total amount of energy scattered by a single scattering process up to the time *t*. This energy is distributed inside a sphere with a radius $r_U = vt$. The total amount of energy scattered up to the time *t* and also distributed inside a sphere with a radius $r_U = vt$ may be easily written as:

$$U_{total}(t) = 1 - \exp\left(-\frac{\omega t}{Q}\right) \tag{2.22}$$

Then, we may write the ratio of the single scattered energy to the total scattered energy up to a time t as:

$$R(t) = \frac{n\sigma vt \exp(-n\sigma vt)}{1 - \exp\left(-\frac{\omega t}{Q}\right)} \tag{2.23}$$

and taking into account the following equalities:

$$l = \frac{1}{n\sigma} = \frac{vQ_C}{\omega} \tag{2.24}$$

we may rewrite the ratio as:

$$R(t) = \frac{\frac{\omega t}{Q} \cdot \exp(-n\sigma vt)}{1 - \exp\left(-\frac{\omega t}{Q}\right)} \tag{2.25}$$

In order to study this expression let us define the following parameter:

$$\xi = \frac{\omega t}{Q} \tag{2.26}$$

Then we rewrite the ratio as:

$$R(\xi) = \frac{\xi \exp(-\xi)}{1 - \exp(-\xi)} \tag{2.27}$$

The ratio takes the following values; $R(0)$=1.0; $R(0.20)$=0.90; $R(0.43)$=0.80; $R(0.67)$=0.70. Let us take as a unit of time the arrival time $t_a = d/v$ (d is the hypocentral distance); then we shall rewrite the time as $n \cdot t_a$. Let us also compute ξ for f=1 Hz and v=3.5 Km/s for several possible values of Q and n. Then, we rewrite ξ as a function of d, n,v and Q:

$$\xi = n \cdot d \cdot \frac{2\pi}{v \cdot Q} \tag{2.28}$$

It might be useful to have d as function of the other parameters: Then using Eq. (2.28):

$$d = \xi \frac{v \cdot Q}{2\pi n} \tag{2.29}$$

Let us calculate now for what distance d is $R(\xi)$=0.9 or $R(\xi)$=0.8 for n=2 and n=3 for several values of Q. From Eq. (2.27) $R(\xi)$=0.9 is verified when ξ = 0.2, and R(ξ)=0.8 is verified when ξ = 0.43. We take. v=3.5 km·s^{-1}.

Results are plotted in table Table 2-1 and represented in Figure 2-6. The table and the figure show the distances (in km) up to which the single scattered energy constitutes the 90% and the 80% of the total radiated energy for several values of the quality factor of the medium. These values indicate that care should be taken when using the single scattering approximation in regions where Q might be a small number.

Q	d (n=2) (km)		d (n=3) (km)	
	$\xi = 0.2$	$\xi = 0.43$	$\xi = 0.2$	$\xi = 0.43$
50	2.7	6.0	1.8	4.0
100	5.6	12.0	3.7	8.0
200	11.1	23.9	7.4	16.0
400	22.3	47.9	14.8	31.9
800	44.6	95.8	29.7	63.9

Table 2-1 Maximum distance up to which the single scattering approximation may be used (v=3.5km/s).

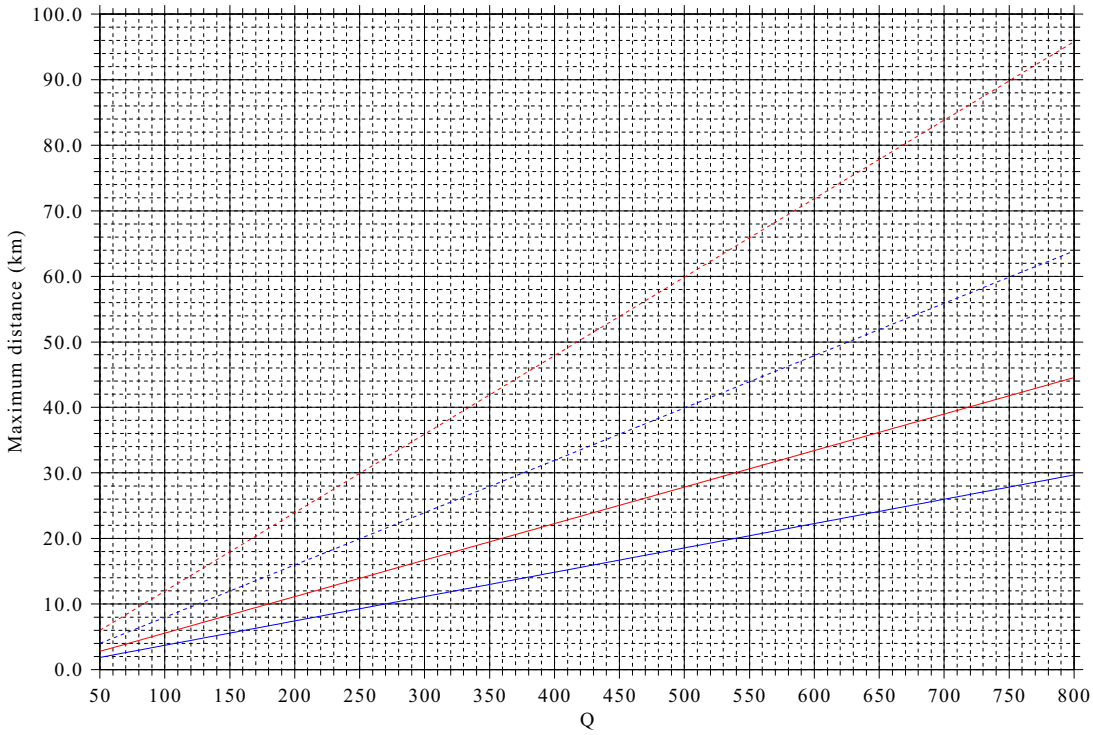

Figure 2-6 Maximum distance up to which the single scattering approximation may be used (v=3.5 km/s). Blue lines correspond to n=2 and red line to n=3. Solid lines correspond to $\xi = 0.2$ and dashed lines to $\xi = 0.43$.

2.4.3 DIFFUSION THEORY

As lapse time increases it is expected that multiple scattering will dominate compared to single scattering. For large lapse times, it is reasonable to assume that direct energy is small and that multiple scattering produces a smooth spatial distribution of energy density. We shall now describe another model in which a strong multiple scattering process can be formulated by means of the diffusion equation (Sato and Fehler, 1998) [10].

Let $E(\mathbf{r},t,\omega)$ be the seismic energy per unit volume within a unit frequency band around ω. Taking into account linear dissipation in the medium, the diffusion equation may be written as:

$$\frac{\partial E}{\partial t} = D \cdot \nabla^2 E - \frac{\omega}{Q} \cdot E \tag{2.30}$$

where D is the diffusivity and the last term represents the loss by anelasticity which

turns the seismic energy into heat. Clearly, here Q is the intrinsic quality factor and does not include the loss by scattering.

The diffusivity D may be related to the wave-scattering process. In analogy with the scattering of particles moving with a certain mean free-path, Dainty et al. [20] obtained the relation between D and the mean free path l as:

$$D = \frac{v \cdot l}{3} \tag{2.31}$$

where v is the velocity of the wave propagation and l is defined as the distance travelled by the primary wave, over which its energy is reduced to e^{-1} by scattering.

The solution of Eq. (2.30) for a point source in time and space is given by:

$$E(\mathbf{r},t,\omega) = \frac{U(\omega)}{(4\pi Dt)^{3/2}} \exp\left(-\frac{r^2}{4Dt}\right) \exp\left(-\frac{\omega t}{Q}\right) \tag{2.32}$$

where $U(\omega)$ is the total seismic energy generated by one earthquake within the unit frequency band around ω. For large t, $\left(t \geq 10 \cdot r^2/4D\right)$ and small distance r at which coda waves are observed, Eq. (2.32) becomes a function of only time and is independent of distance:

$$E(\mathbf{r},t,\omega) = \frac{U(\omega)}{(4\pi Dt)^{3/2}} \exp\left(-\frac{\omega t}{Q}\right) \tag{2.33}$$

The diffusion model solution Eq. (2.33) was used for the analysis of coda recorded near the hypocenter of earthquakes (Wesley, 1965 [19]; Aki and Chouet, 1975 [9]) and the coda of lunar earthquakes (see Figure 2-7) (Nakamura, 1977 [22]; Dainty and Toksöz, 1981 [23]). The energy on the moon is intensely scattered due to the fractured regolith and intrinsic absorption is weak due to the lack of intergranular water.

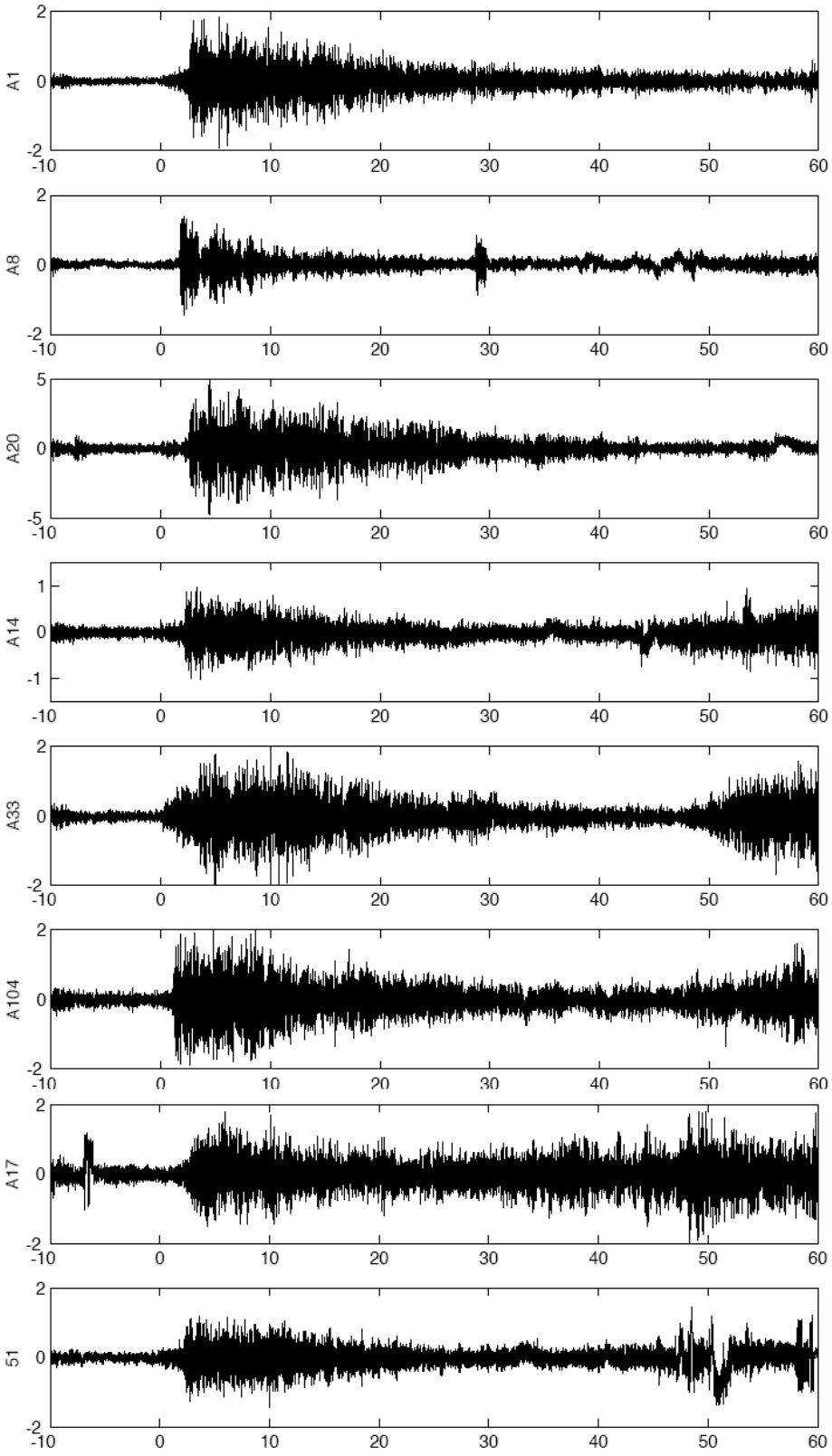

Figure 2-7. Lunar earthquakes [24] showing long coda durations.

2.5 RADIATIVE TRANSFER THEORY

The squared sum of incoherent S-waves that are singly scattered by distributed random heterogeneities can provide an adequate first-order model of the MS envelope of S-wave seismograms. However, as lapse time increases, a greater contribution of higher-order multiple scattering is expected. A systematic approach for modelling the multiple scattering process is to use the radiative transfer theory for the energy density. The equation of radiative transfer is a basic analytical tool in nuclear reactor theory, in the kinetic theory of gases or in electron transport through conducting materials. The theory of radiative transfer discards the phase information contained in individual contributions; actually, this theory focus on the transport of energy, very much like a nuclear physicist is interested in the flux of neutron obtained by summing over individual particles. It is assumed that the addition of power holds rather than the addition of wavefields.

We will define now the fundamental quantities which the subject of Radiative Transfer deals with and derive the basic equation (the equation of radiative transfer) [25]. The solution of this equation will provide us an expression describing the characteristics of the envelope of seismograms and will be useful to evaluate the magnitude of certain important parameters.

2.5.1 RADIATIVE TRANSFER EQUATION

Consider the elemental volume shown in Fig. 1.1 with cross-section da and length ds containing ndads scatterers with n the number density of scatterers. Let the spatially incoherent intensity be defined as the energy per area, per time, and per solid angle $\mathrm{d}\Omega$ so that the energy emergent from this volume in the $\hat{\mathbf{s}}$ direction is $I(s,t)\,\mathrm{d}a\,\mathrm{d}t\,\mathrm{d}\Omega$. The energy a distance ds away, moving at speed c also in the $\hat{\mathbf{s}}$ direction at a time later will be $I(s+\mathrm{d}s,t+\mathrm{d}t)\,\mathrm{d}a\,\mathrm{d}t\,\mathrm{d}\Omega$.

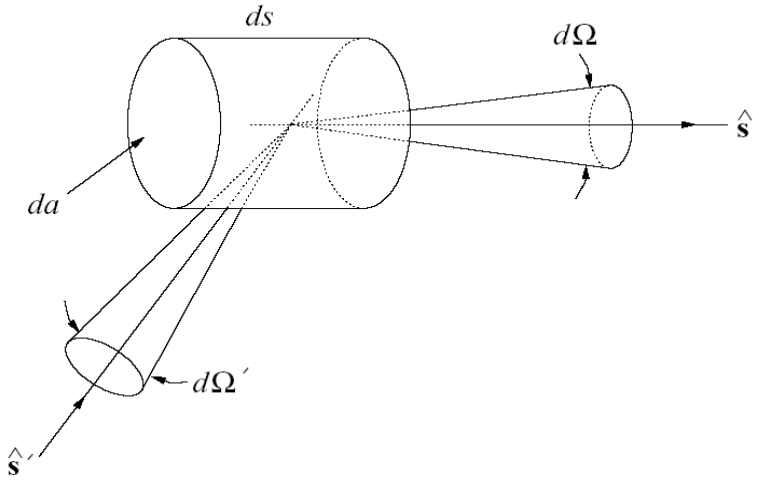

Figure 2-8. Propagation through the scattering volume in the $\hat{\mathbf{s}}$ direction and emission into the $\hat{\mathbf{s}}$ direction from scattering events due to energy from the $\hat{\mathbf{s}}'$ direction [26].

The difference in energy can be attributed to a loss caused by absorption and scattering, and an increase caused by emissions into the direction of propagation from other scattering events or from sources within the medium. This energy balance is written as:

$$I(s+\mathrm{d}s,t+\mathrm{d}t)\,\mathrm{d}a\,\mathrm{d}t\,\mathrm{d}\Omega - I(s,t)\,\mathrm{d}a\,\mathrm{d}t\,\mathrm{d}\Omega = -\eta I(s,t)\,\mathrm{d}a\,\mathrm{d}s\,\mathrm{d}t\,\mathrm{d}\Omega + n\varepsilon(s,t)\,\mathrm{d}a\,\mathrm{d}s\,\mathrm{d}t\,\mathrm{d}\Omega \tag{2.34}$$

where $\eta = n\left(\sigma_s + \sigma_a\right)$ is the total intensity attenuation, σ_a is the absorption cross section per scatterer, σ_s is the scattering cross section per scatterer, and $\varepsilon(s,t)$ is the emission coefficient per scatterer.

The absorption cross section may include absorption within the scatterer as well as dissipation within the medium (which is zero for most applications with electromagnetic waves). The emission coefficient may include emissions from scattering events and primary sources. Equation (2.34) implies that

$$\frac{\partial I(s,t)}{\partial s}\mathrm{d}s + \frac{\partial I(s,t)}{\partial t}\mathrm{d}t = -\eta I(s,t)\,\mathrm{d}s + n\varepsilon(s,t)\,\mathrm{d}s \tag{2.35}$$

Since $\mathrm{d}s = c\,\mathrm{d}t$, Eq. (2.35) becomes:

$$\frac{\partial I(s,t)}{\partial s}+\frac{1}{c}\frac{\partial I(s,t)}{\partial t}=-\eta I(s,t)+n\varepsilon(s,t) \tag{2.36}$$

Note that in the absence of emissions, I(s,t) displaces and attenuates with time in the following manner:

$$I(s,t)=f(s-ct)\exp\left(-\eta ct\right) \tag{2.37}$$

In three dimensions the radiative transfer equation becomes

$$\nabla I(s,t)\cdot\hat{\mathbf{s}}+\frac{1}{c}\frac{\partial I(\mathbf{r},\mathbf{s},t)}{\partial t}=-\eta I(\mathbf{r},\hat{\mathbf{s}},t)+n\varepsilon(\mathbf{r},\hat{\mathbf{s}},t) \tag{2.38}$$

where $\hat{\mathbf{s}}$ is the direction of propagation, $\mathbf{r}$ is the space vector and the total attenuation has been assumed isotropic (*i.e.* independent of $\hat{\mathbf{s}}$).

To find the emission coefficient, consider the same volume of scatterers with radiation incident from the $\hat{\mathbf{s}}'$ direction within the solid angle $d\Omega'$ scattering into the $\hat{\mathbf{s}}$ direction in solid angle $d\Omega$ also shown in Figure 2-8. Let the angular distribution of the scattered portion of the radiation, scattered from the direction into the direction, be defined by

$$q(\hat{\mathbf{s}},\hat{\mathbf{s}}')\frac{d\Omega}{4\pi} \tag{2.39}$$

where $q(\hat{\mathbf{s}},\hat{\mathbf{s}}')$ is the phase function (Chandrasekhar, 1960)[25] and is 4π times the differential scattering cross-section (Ishimaru, 1978, [27]). The phase function is normalized so that

$$\int_{4\pi} q(\hat{\mathbf{s}},\hat{\mathbf{s}}')\frac{d\Omega}{4\pi}=\sigma_s \tag{2.40}$$

which means that for isotropic scattering $q(\hat{\mathbf{s}},\hat{\mathbf{s}}')=\sigma_s$. This angular distribution multiplied by the intensity and integrated over all incoming directions is the emitted radiation per scatterer. Thus in the absence of primary sources the emission coefficient is:

$$\varepsilon(\mathbf{r},t,\hat{\mathbf{s}}) = \int_{4\pi} q(\hat{\mathbf{s}},\hat{\mathbf{s}}')I(\mathbf{r},t,\hat{\mathbf{s}})\frac{d\Omega}{4\pi} \tag{2.41}$$

The full scalar radiative transfer equation is then written as:

$$\nabla I(s,t)\cdot\hat{\mathbf{s}} + \frac{1}{c}\frac{\partial I(\mathbf{r},\mathbf{s},t)}{\partial t} = -\eta I(\mathbf{r},\hat{\mathbf{s}},t) + \int_{4\pi} p(\hat{\mathbf{s}},\hat{\mathbf{s}}')I(\mathbf{r},t,\hat{\mathbf{s}})\frac{d\Omega}{4\pi} \tag{2.42}$$

where $p(\hat{\mathbf{s}},\hat{\mathbf{s}}') = nq(\hat{\mathbf{s}},\hat{\mathbf{s}}')$ is the phase function for an assemblage of independent scatterers. The radiative transfer equation is a first order integro-partial differential equation in space, time, and propagation direction. Its solutions are in general nontrivial.

2.5.2 SOLUTIONS OF THE RADIATIVE TRANSFER EQUATION. ISOTROPIC SCATTERING

Initial seismological models using the radiative transfer theory are those of Wu (1985)[28] and Wu and Aki (1988) [11]. They applied the stationary state solution for media having isotropic scattering. Shang and Gao (1988) [29] first formulated the multiple isotropic scattering process in 2-D space as an integral equation for the nonstationary state for the case of impulsive radiation. Zeng et al. (1991) [30] extended the nonstationary case to 3-D space. Sato et al. (1997) [31] used the radiative transfer theory to investigate the multiple isotropic scattering process for nonspherical source radiation whereas Sato (1994 [32], 1995 [33]) investigated the multiple nonisotropic scattering process in the framework of the radiative transfer theory.

The radiative transfer equation can be solved exactly in the Fourier space [30] in the case of isotropic scattering for one, two, three and four dimensions. It is possible to write an explicit expression in one, two and four dimensions. In three dimensions an accurate interpolation formula can be derived [34].

We will focus in the solutions on the real three-dimensional space. If we consider isotropic scattering, we may rewrite Eq. (2.42) in the following way:

$$\nabla I(s,t)\cdot\hat{\mathbf{s}}+\frac{1}{c}\frac{\partial I(\mathbf{r},\mathbf{s},t)}{\partial t}=-(l^{-1}+l_a^{-1})I(\mathbf{r},\hat{\mathbf{s}},t)+l^{-1}I(\mathbf{r},t)+c^{-1}S(\mathbf{r},t,\hat{\mathbf{s}})$$
$$I(\mathbf{r},t)=\int_{4\pi}I(\mathbf{r},t,\hat{\mathbf{s}})\frac{d\Omega}{4\pi} \tag{2.43}$$

where $l^{-1}=n\sigma_s$ and $l_a^{-1}=n\sigma_a$ and S is a source function.

We notice here that the dependence of the intensity on the absorption is through a $\mathbf{r}$ and $\hat{\mathbf{s}}$ independent factor

$$I(\mathbf{r},t)_{with\ absorption}=I(\mathbf{r},t)_{without\ absorption}\exp\left(-ct/l_a\right) \tag{2.44}$$

Without loss of generality we can, therefore, leave the absorption of our considerations in the following, taking effectively $l_a\to\infty$

The solution will be written as a summation of three terms. The first one corresponds to the ballistic peak. The second one corresponds to the contribution due to single scattering. The last term accounts for multiple scattering.

2.5.2.1 Ballistic peak and single scattering

The ballistic peak consists of a delta function due to unscattered waves:

$$I_0(r,t)=\frac{1}{4\pi r^2}\delta(r-ct)\exp\left(\frac{-ct}{l}\right) \tag{2.45}$$

This peak will be followed by a tail due to waves which have undergone a single forward scattering event. The shape of the tail is given by P_1, which can be computed analytically for any dimension. P_1 has an integrable singularity at $r=ct$, which adds a tail to the ballistic peak. The singularity is logarithmic:

$$I_1(r,t)=\frac{1}{4\pi lctr}\exp\left(\frac{-ct}{l}\right)\ln\left(\frac{ct+r}{ct-r}\right) \tag{2.46}$$

2.5.2.2 Multiple scattering

The contribution coming from multiple scattering is usually written as the summation of two terms. In this way the corresponding integrals may be evaluated by means of numerical integration techniques. The first term corresponds to double scattering:

$$I_2(r,t)=\frac{1}{16\pi l^2}\exp\left(-\frac{ct}{l}\right)\left[\frac{\pi^2}{ct}-\frac{3}{r}\int_0^{r/ct}\left(\ln\left(\frac{1+\alpha}{1-\alpha}\right)\right)^2 \mathrm{d}\alpha\right] \tag{2.47}$$

and the other terms correspond to multiple scattering (excluding double scattering):

$$\sum_{N\geq 3} P_n(r,t)=\frac{1}{4\pi^3 r l^3}\int_{-\infty}^{+\infty}\frac{\exp(i\Omega ct)}{2}\mathrm{d}\Omega\int_0^{\infty}\frac{1}{k^2}\frac{\left[\arctan\left(\dfrac{k}{1/l+i\Omega}\right)\right]^4}{\left[k-\dfrac{1}{l}\arctan\left(\dfrac{k}{1/l+i\Omega}\right)\right]}\mathrm{d}k \tag{2.48}$$

This is the expression that Passchenns [34] obtained. The expression derived by Zeng [30] including absorption may be written as:

$$\sum_{N\geq 3} P_n(r,t)=\frac{1}{4\pi^3 r l^3}\int_{-\infty}^{+\infty}\frac{\exp(i\Omega ct)}{2}\mathrm{d}\Omega\int_0^{\infty}\frac{1}{k^2}\frac{\left[\arctan\left(\dfrac{k}{1/l+1/l_a+i\Omega}\right)\right]^4}{\left[k-\dfrac{1}{l}\arctan\left(\dfrac{k}{1/l+1/l_a+i\Omega}\right)\right]}\mathrm{d}k \tag{2.49}$$

This expression also verifies Eq. (2.44). Actually, it possible to define a new variable Ω' such that:

$$\begin{aligned} i\Omega &= i\Omega' - 1/l_a \\ \Omega &= \Omega' + i/l_a \end{aligned} \tag{2.50}$$

It is then easily demonstrated that both solutions are identical.

2.5.2.3 Analytical approximation of multiple scattering integrals

It is possible to derive accurate analytical expressions to compute the integrals corresponding to Eq. (2.47) and Eq. (2.48). The solution may then be written (with accuracy within 2% out of the ballistic peak):

$$I(r,t) \simeq \frac{1}{4\pi r^2}\delta(r-ct)\exp\left(\frac{-ct}{l}\right) + \frac{\left(1-r^2/c^2t^2\right)^{\frac{1}{8}}}{\left(4\pi l\, ct/3\right)}\exp\left(\frac{-ct}{l}\right)G\left(\frac{ct}{l}\left[1-\frac{r^2}{c^2t^2}\right]^{\frac{3}{4}}\right) \tag{2.51}$$

$$G(x) = 8(3x)^{-3/2}\sum_{N=1}^{\infty}\frac{\Gamma\left(\frac{3}{4}N+\frac{3}{2}\right)}{\Gamma\left(\frac{3}{4}N\right)}\frac{x^N}{N!}$$

Where it is possible to approximate G(x) as follows

$$G(x) \simeq \exp(x)\sqrt{1+2.026/x} \tag{2.52}$$

All these expressions are useful in the calculation of I^{-1} and I_a^{-1} [13].

2.5.2.4 Comparing exact solutions and approximate solutions

The only way to compare the analytical approximate solution an the exact solution is to carry out a numerical integration of the double integral in Eq. (2.48). This integral is a difficult one because of the following reasons:

i. The integrand is highly oscillatory

ii. The integrand logarithmically diverges in the limits of integrations.

It is possible to use the Fast Fourier Transform (FFT) [35-36] algorithm to evaluate the integral. FFT algorithm may not be an accurate algorithm when the integrand is highly oscillatory. In such a case aliasing effects may arise and the accuracy of the calculation may be low.

To avoid this problem, Paasschens [34] develops real integrals in order to facilitate the numerical inversion of the Fourier Transform in Eq. (2.48). We could not obtain the exact result from that development. We used several cubature algorithms (included the ones described in the next paragraphs) but all of them gave us a wrong solution. We were not able to tell if the error was originated because of a wrong evaluation of the integral by numerical algorithms or because there is a typographic mistake in the Paasschens development. Certainly, the evaluation of two-dimensional integrals is a non-trivial problem, especially if the integrand shows a strong oscillatory behaviour and

also diverges in some regions.

Then we decided to obtain the exact solution directly from Eq.(2.48) using powerful numerical algorithms. We finally used two different algorithms, a two-dimensional adaptative cubature algorithm called Cubpack [37] and a non-adaptive algorithm r2d2lri [38]. These algorithms employ very different strategies for automatic integral evaluation. [39]. Then, if both methods give us the same result this will indicate that we are on the right way. A short description of both methods follows.

Cubpack employs a globally adaptative algorithm that uses successive refinements or subdivisions of the integration region (IR) where each subdivision is used to provide a better approximation to the integral. These subdivisions are designed to dynamically concentrate the computational work in the subregions of IR where the integrand is most irregular, and thus to adapt to the behaviour of the integrand. The general structure of the globally adaptive algorithm consists of a sequence of stages. Each stage has the following five main steps:

i. Select a subregion with largest estimated error from the current set of subregions.

ii. Divide the selected subregion.

iii. Apply a local cubature rule to any new subregions.

iv. Update the subregion set.

v. Update the global integral and error estimates, and check for termination.

The initial subregion set for the algorithm is the original collection of simplices (*n*-dimensional triangles) of IR. The required input for such an algorithm is IR, the integrand, a limit on the number of integrand values allowed, and a requested error tolerance. The algorithm terminates when the estimated global error is less than the one requested or further subdivision would require too many function evaluations.

r2d2lri is a non-adaptive algorithm implemented in C++ for performing automatic cubature over a wide variety of finite and non-finite two-dimensional domains. The core integrator of *r2d2lri()* evaluates cubatures over the domain $[0,1]^2$ using a non-adaptive

sequence of embedded lattice rules, coupled with a sixth-order Sidi transformation (a type of variable transformation for numerical integration). Before any cubature is performed, the provided integral is automatically transformed onto $[0,1]^2$. Since different types of non-finite to finite domain transformations suit different forms of integrand behaviour, for non-finite domains, *r2d2lri* performs cubatures using an ordered succession of up to three different transformations onto $[0,1]^2$ until it is determined that the requested accuracy (or the best achievable result) has been attained.

These methods allow to carry out integrations over real integrands. Notice that the integral in Eq. (2.48) has to be a real number since it corresponds to an addition of multiple scattered energies. Using the following identity:

$$\arctan(z) = \frac{i}{2}\ln\left(\frac{i+z}{i-z}\right) \tag{2.53}$$

it is possible to easily devise an algorithm to compute the real part of the integrand.

To check the accuracy of Eq. (2.51) and Eq. (2.52) we now compare with a numerical evaluation of Eq.(2.46), Eq. (2.47) and Eq.(2.48) in Figure 2-9. Eq. (2.47) may be evaluated with a standard one-dimensional integration algorithm as the Romberg algorithm [46]. Eq.(2.48) will be evaluated using Cubpack++ and r2d2lri algorithms. Both algorithms will provide almost identical results. Only the ones obtained with Cubpack++ will then be plotted. Also, the diffusive approximation in Eq.(2.32) is considered in the figure.

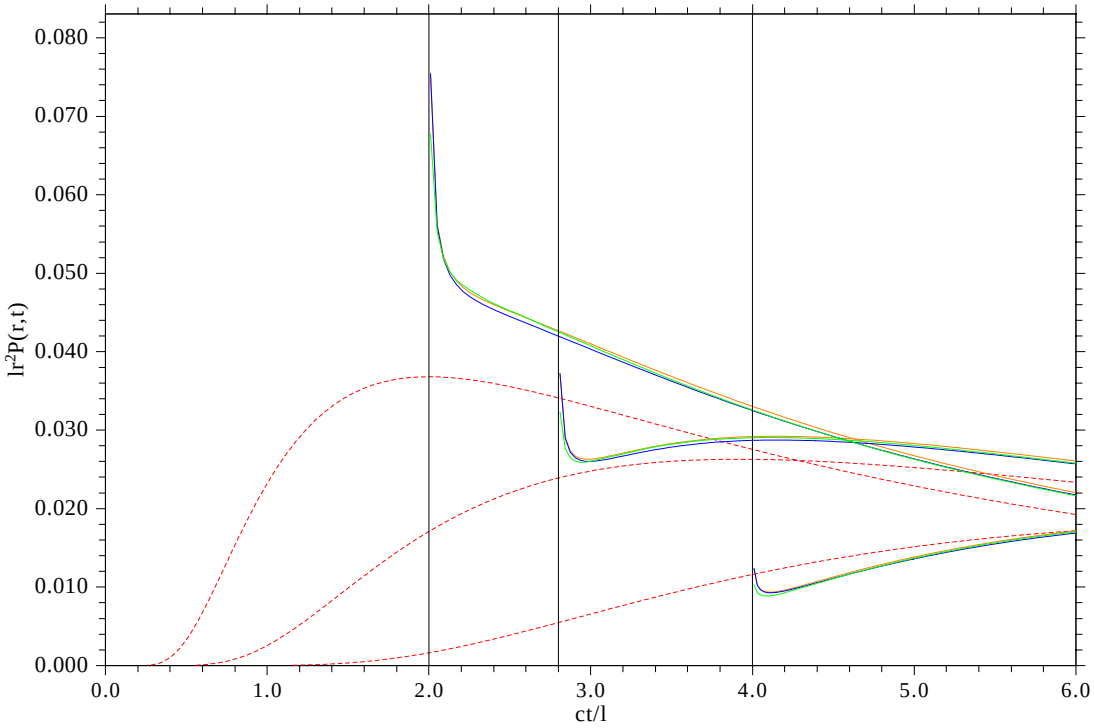

Figure 2-9. Intensity as a function of time t, at distances $r = 2.0l,\ 2.8l$ and $4.0l$, from left to right. The blue lines are the exact result, which is very close to the interpolation formulas: green line corresponds to Eq. (2.51) and orange line corresponds to using the approximation in Eq. (2.52). Dashed red lines correspond to the Gaussian diffusive result.